



HAL
open science

Temporal evolution of age data under transient pumping conditions

Sarah Leray, Jean-Raynald de Dreuzy, Luc Aquilina, Virginie Vergnaud-Ayraud, Thierry Labasque, Olivier Bour, Tanguy Le Borgne

► **To cite this version:**

Sarah Leray, Jean-Raynald de Dreuzy, Luc Aquilina, Virginie Vergnaud-Ayraud, Thierry Labasque, et al.. Temporal evolution of age data under transient pumping conditions. *Journal of Hydrology*, 2014, 511, pp.555-566. 10.1016/j.jhydrol.2014.01.064 . insu-00952724

HAL Id: insu-00952724

<https://insu.hal.science/insu-00952724>

Submitted on 28 Feb 2014

HAL is a multi-disciplinary open access archive for the deposit and dissemination of scientific research documents, whether they are published or not. The documents may come from teaching and research institutions in France or abroad, or from public or private research centers.

L'archive ouverte pluridisciplinaire **HAL**, est destinée au dépôt et à la diffusion de documents scientifiques de niveau recherche, publiés ou non, émanant des établissements d'enseignement et de recherche français ou étrangers, des laboratoires publics ou privés.

1 Temporal evolution of age data under transient pumping conditions

2 Authors: Leray S.^{1,*,#}, de Dreuzy J.-R.^{1,2}, Aquilina L.¹, Vergnaud-Ayraud V.¹, Labasque T.¹,
3 Bour O.¹, Le Borgne T.¹.

4

5 ¹ Géosciences Rennes (UMR 6118 CNRS), Université de Rennes 1, Campus de Beaulieu,
6 35042 Rennes cedex, France

7 ² IDAEA (CSIC), c/ Jordi Girona, 08034, Barcelona, Spain

8 *Corresponding author: sarah.leray1@gmail.com

9 # Now at: IFP Energies nouvelles, 1-4, avenue de Bois-Préau, 92852 Rueil-Malmaison,
10 France

11

12 **Key words:** groundwater age, residence time distribution, environmental tracers,
13 chlorofluorocarbons, heterogeneous aquifers, transient flow conditions

14

15 **Abstract**

16 While most age data derived from tracers have been analyzed in steady-state flow conditions,
17 we determine their temporal evolution when starting a pumping. Our study is based on a
18 model made up of a shallowly dipping aquifer overlain by a less permeable aquitard
19 characteristic of the crystalline aquifer of Plœmeur (Brittany, France). Under a pseudo
20 transient flow assumption (instantaneous shift between two steady-state flow fields), we solve
21 the transport equation with a backward particle-tracking method and determine the temporal

22 evolution of the concentrations at the pumping well of CFC-11, CFC-12, CFC-113 and SF₆.
23 Apparent ages evolve because of the modifications of the flow pattern and because of the non-
24 linear evolution of the tracer atmospheric concentrations. To identify the respective role of
25 these two causes, we propose two successive analyses. We first convolute residence time
26 distributions initially arising at different times at the same sampling time. We secondly
27 convolute one residence time distribution at various sampling times. We show that flow
28 pattern modifications control the apparent ages evolution in the first pumping year when the
29 residence time distribution is modified from a piston-like distribution to a much broader
30 distribution. In the first pumping year, the apparent age evolution contains transient
31 information that can be used to better constrain hydrogeological systems and slightly
32 compensate for the small number of tracers. Later, the residence time distribution hardly
33 evolves and apparent ages only evolve because of the tracer atmospheric concentrations. In
34 this phase, apparent age time-series do not reflect any evolution in the flow pattern.

35 1. Introduction

36 Groundwater flow is by nature transient, because of the temporal variations of boundary
37 conditions such as the variations of recharge over different time scales (seasons, decades,
38 centuries or more) and because of anthropogenic forcings such as pumping or artificial
39 recharge. Pumping has a significant impact on the flow pattern and on solute transport. They
40 induce more convergent flow pattern and, even in some cases, some extension of recharge
41 areas (Bredehoeft, 2002; Frind et al., 2005). It will as well speed up flows and modify the
42 relative role of structures, hydrodynamic properties and boundary conditions – increasing for
43 instance the effective recharge rate of unconfined aquifers in close connection to the surface
44 (Leray et al., 2012; Sophocleous, 2005).

45 Environmental tracers have been widely used for water sources identification, estimation of
46 residence time distribution and model calibration amongst others (Castro et al., 1998; Cook et
47 al., 2005; Long and Putnam, 2009; McMahon et al., 2010; Stichler et al., 2008). Because they
48 integrate velocities along flow paths, they reflect flow conditions over various time scales in
49 the past. They are sensitive to transient phenomena affecting the flow field. More precisely,
50 they are sensitive to transient phenomena occurring over time scales comparable to their
51 characteristic time (Zuber et al., 2011).

52 Yet, the influence of transient flow conditions on environmental tracer concentration has
53 hardly been addressed. Sanford et al. (2004) have reconstructed transient recharge rates using
54 ^{14}C data in the regional alluvial middle Rio Grande Basin. Schwartz et al. (2010) have noticed
55 that the interpretation of ^{14}C age in transient flow models can be ambiguous in terms of flow
56 pattern as data distributed over the aquifer reflect different flow conditions. Long and Putnam
57 (2009) have incorporated CFCs and ^3H data from a karstic system in binary mixing model
58 with dilution allowing parameters to vary with time. Fewer studies have analyzed the role of
59 transient flow conditions on residence time distribution. Using numerical simulations,
60 Troldborg et al. (2008) have showed the effect of recharge seasonality on residence time
61 distribution and have noticed distinct behaviors. In the shallowest part of the studied
62 heterogeneous aquifer, residence times tend to be smaller than in steady-state flow conditions
63 while they tend to be higher in the deepest part of the aquifer. The effect in a fully-penetrating
64 well is however negligible. Zinn and Konikow (2007) have analyzed the effect of the start of
65 pumping on a synthetic configuration composed of an aquifer overlain by an aquitard. Their
66 study have revealed important changes of the mean residence time at the pumping well and of
67 the residence time distribution over long periods of time. Changes only come from the

68 modification of the flow pattern as they solely focused on the mean residence time and not on
69 the apparent ages obtained from tracers.

70 In this study, we determine the influence of the transient groundwater flow pattern induced by
71 anthropogenic forcing on environmental tracers concentrations (CFC-11, CFC-12, CFC-113
72 and SF₆) interpreted in apparent ages. We consider that the transient flow pattern is induced
73 by the instantaneous start of a pumping well. Tracer concentrations are reported at the
74 pumping well. Our study is based on the hydrogeological setting of Plœmeur, which is a well
75 documented aquifer where water has been produced for the last two decades for the water
76 supply of the nearby city (Le Borgne et al., 2004; Le Borgne et al., 2006; Ruelleu et al., 2010;
77 Touchard, 1999). Although based on a specific site, the results of this study can be
78 generalized to shallowly dipping aquifers overlain by a leaking layer. Such condition has been
79 proved to be of importance for groundwater resources in hard-rock aquifers (Leray et al.,
80 2013). While our objective is more methodological than targeted to a specific site, the
81 Plœmeur aquifer still offers a complex and yet realistic hydrodynamic context. We use
82 hydrogeological models previously calibrated in steady-state flow conditions under pumping
83 (Leray et al., 2012) and determine the effect of transient flow conditions on apparent ages. We
84 first aim at determining the causes of the temporal evolution of the apparent ages and
85 specifically when they rather come from the transient modifications of the flow pattern and
86 when they are more linked to the specificities of the tracers, especially their atmospheric
87 concentrations. We second aim at assessing the interest of age data time series for models
88 segregation. After recalling in section 2 the hydrogeological, flow and transport models, we
89 present the results in section 3 and discuss them in section 4.

90 2. Hydrogeological, flow and transport models

91 We successively describe the hydrogeological models of the Plœmeur site that will be used as
92 a basis of this study, the flow and the transport models as well as the numerical methods used.
93 We finally comment in details the derivation of the tracer concentrations and the
94 corresponding apparent ages to highlight the possible causes of apparent age temporal
95 variations.

96 2.1. Hydrogeological model

97 The study of the effects of transient flow conditions, induced by pumping, on age data is
98 based on the Plœmeur aquifer, a highly heterogeneous hard-rock aquifer located on the south
99 coast of Brittany near the city of Lorient (France). A previous study based on the inversion of
100 gravimetric data has established a geological conceptual model (Ruelleu et al., 2010). This
101 conceptual model is composed of two transmissive structures at large scale, the dipping
102 contact zone and a North 20° normal fault, besides the Plœmeur and Guidel granites and
103 overlying micaschists acting as a typical aquitard. Local heterogeneities are not represented in
104 the model. The supplying area to the pumping well which amounts to a few square kilometers
105 is limited in the North-South direction by these two granites. The pumping rate thus has a
106 strong impact on flow pattern within this heterogeneous aquifer.

107 Because the shape and the dip of the contact zone are only partially known, the overall
108 thickness of the aquitard-aquifer system remains relatively uncertain. To account for this
109 uncertainty, a few structural models with distinct thickness have been built (Figure 1 and
110 Table 1). The hydraulic properties of the different rocks have been set either to common
111 values as for the granites which are found almost impervious (10^{-11} m/s), or to measured
112 values as for the micaschists (10^{-7} m/s – 5×10^{-6} m/s) and the contact zone (1.9×10^{-3} m²/s –

113 $3 \times 10^{-3} \text{ m}^2/\text{s}$). In addition, the potential recharge rate R has been estimated at 200 mm per year
 114 (Carn, 1990; Leray et al., 2012; Touchard, 1999). Following these constraints, each model has
 115 been calibrated against the mean piezometric level measured at the pumping well (-5.5 masl)
 116 in steady-state flow under pumping conditions (Leray et al., 2012) by slightly adjusting the
 117 contact zone transmissivity previously estimated from long-term pumping tests (Le Borgne et
 118 al., 2006). Uniform porosity has also been calibrated against the CFC-12 age (30 years \pm 1
 119 year in 2009). Note that the overall volume of the system is about $1.5 \times 10^9 \text{ m}^3$ and the mean
 120 residence time of the model – *i.e.* the first moment of the residence time distribution – is
 121 around 13 years in ambient conditions and 50 years in pumping conditions. .

122 Our study has been carried out on about ten representative hydrogeological models differing
 123 by their structure, their micascists permeability and their porosity. The interest of
 124 considering different models is to investigate the potential influence of the hydrogeological
 125 structure on the apparent ages and their evolution. We discuss further in section 4 how this
 126 sensitivity might be useful as an additional way to characterize the flow pattern. Among this
 127 set of models, only two are used here to illustrate the methodology as they all lead to the same
 128 conclusions. Table 1 synthesizes the parameters of the two chosen hydrogeological models.

129 2.2. Flow model

130 Transient flow conditions are induced by starting a pumping well. The transient pumping rate
 131 $Q_w(t)$ is a step function going from zero before the starting date t_{switch} , to a positive value Q_p :

$$Q_w(t) = \begin{cases} 0 & t \leq t_{switch} \\ Q_p & t > t_{switch} \end{cases} \quad (1)$$

132 In the particular case of the site of Plœmeur, Q_p is set at $3.36 \times 10^{-2} \text{ m}^3/\text{s}$. Pumping started in
 133 1991 and the most part of the evolution of the piezometric levels occurred only in a few years
 134 after the start of pumping. t_{switch} has thus been set at 1994. We solve the 3D diffusivity
 135 equation for the hydraulic head $h(\mathbf{x}, t)$ with free surface boundary conditions under a pseudo
 136 transient flow approximation:

$$\nabla \cdot (K(\mathbf{x}) \nabla h(\mathbf{x}, t)) = 0 \quad (2)$$

$$\left. \begin{array}{l} K(\mathbf{x}) \nabla h(\mathbf{x}, t) \cdot \mathbf{n} = -R \quad \& \quad h(\mathbf{x}, t) = z(\mathbf{x}) \\ h = z_{\text{ground}} \end{array} \right\} \begin{array}{l} \text{where } h < z_{\text{ground}} \\ \text{anywhere else} \end{array} \quad \text{on } \Gamma_s \quad (3)$$

$$\nabla h(\mathbf{x}) \cdot \mathbf{n} = 0 \quad \text{on } \Gamma_{\text{west}} \text{ and } \Gamma_{\text{east}} \quad (4)$$

$$h(\mathbf{x}) = z_{\text{ground}} - z_0 \quad \text{on } \Gamma_{\text{north}} \text{ and } \Gamma_{\text{south}} \quad (5)$$

$$\int_{\Gamma_w} K(\mathbf{x}) \nabla h(\mathbf{x}, t) \cdot \mathbf{n}_w \, d\Gamma_w = Q_w(t) \quad \text{sink term} \quad (6)$$

137 where $K(\mathbf{x})$ is the hydraulic conductivity; \mathbf{n} is the outgoing normal to the saturated domain; R
 138 is the potential recharge rate; z_{ground} is the ground surface elevation; Γ_s is the top of the
 139 saturated domain; Γ_{west} , Γ_{east} , Γ_{north} and Γ_{south} are respectively the West, East, North and South
 140 sides of the domain; z_0 is a reference height; \mathbf{n}_w is the ingoing normal to the well screen; Γ_w is
 141 the well screen surface and $Q_w(t)$ is the transient pumping rate defined in equation 1 and
 142 located at \mathbf{x}_w . The pseudo transient approximation intervenes in equation 6 and consists in
 143 assuming that steady-state flow conditions are quickly established compared to the solute

144 transport evolution. This is a reasonable approximation of transient flow conditions valid at
145 low specific storage and with the advantage of being less costly numerically. Practically, it
146 consists in ignoring the transition between the two steady-state velocity fields under ambient
147 and pumping conditions.

148 Equation 2 is solved in unconfined conditions since seepage conditions are *a priori* not
149 known. Unconfined conditions are satisfied through both conditions at the free surface
150 boundary of equation 3. When the free surface level is below the ground surface level, the
151 effective recharge rate is equal to the potential recharge rate R ; anywhere else, the free surface
152 level is set at z_{ground} and the effective recharge rate continuously evolves from negative values
153 in the discharge zone to positive potential recharge rate R . The model has been built to
154 include the nearest watersheds both in ambient and pumping conditions in order to minimize
155 the potential effects of the boundary conditions. No-flow conditions applied on the West and
156 East boundaries (Equation 4, Figure 2) do not have any impact on the recharge areas captured
157 by the pumping zone located at depth in the pumping well. Imposed heads, set at depth z_0 (5
158 meters below the ground surface level), are applied to the South and the North boundaries
159 without any significant influence on the system because of the almost impervious granites
160 (Equation 5, Figure 2).

161 2.3. Transport model

162 Transport is considered only advective as the macro-scale dispersion from local dispersion
163 and diffusion is assumed to have a much smaller effect compared to the macro-scale
164 dispersion induced by structural heterogeneity and sampling (LaBolle and Fogg, 2001).
165 Transport is modeled by the advection equation (Bear, 1991; de Marsily, 1986):

$$\frac{\partial C(\mathbf{x}, t)}{\partial t} + \nabla \cdot \left(\frac{\mathbf{q}(\mathbf{x}, t)}{\theta} C(\mathbf{x}, t) \right) + \frac{Q_w(t) C_w(t)}{\theta} = 0 \quad (7)$$

$$C(\mathbf{x}, t = 0) = C_0(\mathbf{x}) \quad (8)$$

$$C(\mathbf{x}, t) = C_1(t) \quad \text{on } \Gamma_1 \quad (9)$$

166 with $C(\mathbf{x}, t)$ the solute concentration at the position \mathbf{x} and at the time t ; θ the effective porosity;
 167 $Q_w(t)$ the rate of the pumping well; $C_w(t)$ the solute concentration at the pumping well; $C_0(\mathbf{x})$
 168 the initial condition; $C_1(t)$ is the boundary condition on a first-type boundary (Γ_1) - such as the
 169 tracer atmospheric concentration at the free surface boundary - and $\mathbf{q}(\mathbf{x}, t)$ the pseudo transient
 170 Darcy's flux derived from the head field $h(\mathbf{x}, t)$:

$$\mathbf{q}(\mathbf{x}, t) = -K(\mathbf{x}) \nabla h(\mathbf{x}, t). \quad (10)$$

171 2.4. Numerical methods

172 The unconfined flow equations are solved using a computationally effective finite-volume
 173 approach with a local adaptation scheme (Bresciani et al., 2011). The advection equation is
 174 solved in backward-time that consists in reversing the flow field and adapting the boundary
 175 conditions (Neupauer and Wilson, 1999; Neupauer and Wilson, 2001; Neupauer and Wilson,
 176 2002). To solve the transport equation, we use a Lagrangian random walk method well-suited
 177 to purely advective transport (de Dreuzy et al., 2007; Kinzelbach, 1988) and adapted to the
 178 unconfined conditions and to the backward-time resolution. We inject particles proportionally
 179 to flow (Kreft and Zuber, 1978) at the pumping well cell and tracked them to the aquifer free

180 surface. The chosen number of injected particles (5×10^6) is determined through a convergence
 181 test of the mean and the variance of the residence time distribution. Flow and transport
 182 simulations are carried out using the H2OLAB platform (Bresciani et al., 2011; Erhel et al.,
 183 2008; Erhel et al., 2009).

184 2.5. Computation and temporal evolution of apparent age

185 We derive the residence time distribution $p(t)$ from the equally likely residence times given by
 186 the particles. The mean concentration C_w of a tracer at the pumping well and at the sampling
 187 date t_w is determined by the convolution of the residence time distribution $p(t)$ with the
 188 atmospheric concentration $C_{in}(t_w - t)$ of the tracer (Kreft and Zuber, 1978; Maloszewski and
 189 Zuber, 1982):

$$C_w = \int_0^{+\infty} C_{in}(t_w - t)p(t)dt = \int_{-\infty}^{t_w} C_{in}(t)p(t_w - t)dt. \quad (11)$$

190 Note that, to highlight that the residence time distribution $p(t)$ is highly dependent on a given
 191 sampling date t_w , we later use it as $p(t_w - t)$ where $t_w - t$ represents the date at which water
 192 recharged, rather than as a function of the residence time “ t ” alone. Throughout the paper,
 193 $p(t_w - t)$ is named recharge date distribution. The apparent age A (Nir, 1964) of a tracer at the
 194 pumping well x_w and at the sampling date t_w is then obtained from the difference between t_w
 195 and the date at which the concentration C_w is equal to the atmospheric concentration:

$$A(t_w) = t_w - C_{in}^{-1}(C_w) = t_w - C_{in}^{-1}\left(\int_{-\infty}^{t_w} C_{in}(t)p(t_w - t)dt\right), \quad (12)$$

196 with C_{in}^{-1} the reciprocal function of the atmospheric concentration.

197 Equation 12 shows the two possible causes of the variation of age A with the sampling date t_w .
198 The first cause is the evolution of the recharge date distribution $p(t_w - t)$ because of the
199 modification of flow conditions that can be traced back to equation 1 through equations 2-11.
200 The shift from ambient to pumping conditions does not only change the flow magnitude but
201 also the flow pattern, the recharge and discharge locations as well as the water mixing within
202 the radius of action of the well (Bredehoeft, 2002). This first cause is solely linked to the flow
203 conditions and does not depend on the tracer characteristics.

204 The second cause of the age variation directly comes from the tracer atmospheric
205 concentration $C_{in}(t)$ through the convolution of equation 11. The non-linear temporal
206 evolution of $C_{in}(t)$ modifies the sampling of the recharge date distribution $p(t_w - t)$. Monotonic
207 and steep evolutions of $C_{in}(t)$ characteristic of the SF_6 and CFCs approximately between the
208 1970s and 1990s results in a large range of weights of the residence times in this period.
209 Flatter evolutions characteristic of the CFCs after the early 1990s give a higher but more
210 equilibrated contribution of the shorter residence times. Depending on the sampling date t_w ,
211 this equilibrated contribution is more or less significant. This effect occurs both in transient
212 and steady-state flow conditions (Trolborg et al., 2008; Waugh et al., 2003; Zhang, 2004).
213 Even under steady-state flow conditions, the non-linear evolution of the atmospheric
214 concentration $C_{in}(t)$ lets the sampled concentration evolve. Under simpler terms, the evolution
215 of the sampled concentration does not only come from the evolution of the system but also
216 from the modification of the "observation device" (C_{in}).

217 It should be noted that this second effect is irrelevant when mixing is minimal like within the
218 framework of the piston-flow model. In such cases, the residence time distribution resumes to
219 a Dirac and the dependency to the tracer atmospheric concentration vanishes in equation 12
220 because of the direct transformation of C_{in} by C_{in}^{-1} . This effect is, however, very relevant

221 close to the aquifer discharge zones (springs, wells) where the mixing of flow paths is
222 maximal. The mixing of sampled flow lines enhances the importance of the non-linear
223 evolution of $C_{in}(t)$. The case studied here pertains more to this second situation, in which,
224 finally, both the temporal evolutions of the recharge date distributions $p(t_w - t)$ and the tracer
225 atmospheric concentration $C_{in}(t)$ can modify the sampled concentration and the derived age
226 $A(t_w)$ (equation 12).

227 To analyze the temporal evolution of the apparent ages, we have determined them using
228 equation 12 by convoluting the recharge date distributions $p(t_w - t)$ obtained under the pseudo
229 transient conditions with the CFC-11, CFC-12, CFC-113 and SF₆ atmospheric concentrations
230 at the evolving sampling dates t_w^i from 1994 to 2009 (Table 2). These dates correspond to
231 sampling 0 to 15 years after the change of flow conditions from ambient to pumping
232 conditions occurring at $t_{switch} = 1994$.

233 3. Results

234 This section first reports the temporal evolution of the apparent ages at the pumping well for
235 the hydrogeological model numbered 1 of the site of Plœmeur described in section 1 and in
236 Table 1. It then analyses the respective effects of the modification of the flow pattern and of
237 the evolution of the tracer atmospheric concentration. The implication of the temporal
238 evolution of the apparent ages for models segregation is further discussed in section 4.1 by
239 comparing the results of the models numbered 1 and numbered 2.

240 3.1. Temporal evolution of apparent age

241 Figure 3 shows the evolution of the apparent ages from CFC-11, CFC-12, CFC-113 and SF₆
242 concentrations with the sampling date t_w ranging from 1994 (ambient conditions) to 2009

243 (Table 2). At first sight, the apparent ages increase first sharply after the start of pumping and
244 then more smoothly whatever the tracer. We indeed expect that the modifications of flow are
245 maximal just after the start of the pumping and later decrease. Though similar, the apparent
246 ages derived from the CFCs and SF₆ still exhibit some differences induced by the tracer
247 atmospheric concentration $C_{in}(t)$. The temporal evolution is minimal for SF₆ because of the
248 almost linear increase of its atmospheric concentration and maximal for the CFC-11 and
249 CFC-12 because of the strong and non-monotonic variations of their atmospheric
250 concentration (IAEA, 2006). CFC-11 and CFC-12 display similar variations because of the
251 similar shapes of their atmospheric concentration chronicles.

252 The increase of the apparent ages in the models considered here is somehow counterintuitive.
253 Indeed, in the exponential model (Haitjema, 1995), the residence time distribution is
254 independent of the pumping rate. Besides, in the piston-flow model, as said in section 2.5,
255 apparent ages remain constant whatever the sampling dates due to minimal mixing. When
256 starting a pumping in those conditions, one would expect an increase of velocity that would
257 directly reduce the residence time and then the apparent ages. In the more complex system
258 modeled here, pumping has a nontrivial effect on the apparent ages. Further insight is given
259 by the analysis of the recharge date distribution $p(t_w - t)$ and its temporal evolution. Figure 4
260 shows the recharge date distribution sampled at three different dates : (a) at $t_w^1 = 1994$ under
261 ambient flow conditions, (b) at $t_w^2 = 1994.1$ approximately one month after the pumping
262 started and (c) at $t_w^3 = 1995$ one year after the pumping started. At later dates ($t_w \geq 1995$),
263 distributions stop to evolve. Therefore, only the distribution at $t_w^3 = 1995$ is displayed.

264 For $1994 \leq t_w \leq 1995$, the system is strongly transient (Figure 4a and b). The start of
265 pumping induces a modification of the recharge date distribution from a narrow piston-like
266 distribution at ambient conditions (t_w^1) (Figure 4a) to a much broader, more exponential-like,
267 later (Figure 4c). Intermediary distribution shapes occur in the first pumping year (Figure 4b).
268 The broadening of the distribution comes from the shift of status of the sampling zone. Under
269 ambient flow conditions, it is a standard zone within the aquifer broken through by just a few
270 flow lines. The different tracers then lead to very close ages (Figure 3). Under pumping
271 conditions, it becomes the major discharge zone of the aquifer focusing a dense net of flow
272 lines that initially discharged in much larger areas such as wetlands (Figure 2) and apparent
273 ages from the different tracers spread out. For $t_w \geq 1994.1$, the recharge date distribution
274 broadens including both shorter and larger residence times than the ambient distribution. In
275 the case of the Plœmeur site, shorter residence times eventually control the apparent ages.
276 This is also consistent with the increase of the mean effective recharge rate and the induced
277 circulation speed up (from 160 mm/year in ambient conditions to 200mm/year in pumping
278 conditions). As previously noted, the distributions sampled in 1995 and later are almost
279 identical. Thus, for $t_w \geq 1995$, sampled concentrations are likely to be more influenced by
280 the temporal evolution of the tracer atmospheric concentrations $C_{in}(t)$ and less by the
281 evolution of the recharge date distribution.

282 3.2. Effect of the temporal evolution of the recharge date 283 distribution

284 3.2.1. Methodology

285 To assess the role of the temporal evolution of the recharge date distribution ($p(t_w - t)$ in
 286 equation 12), we filter out the evolution of the tracer atmospheric concentration ($C_{in}(t)$ in
 287 equation 12). To this end, we translate the distributions $p_i(t_w^i - t)$ (Table 2) to the same
 288 sampling date t_w^t , the exponent “t” standing for translated. The recharge date distributions
 289 $p_i(t_w^i - t)$ are shifted along the date axis by a translation of $t_w^t - t_w^i$ without any
 290 modification of their shape. The shifted distributions are noted $p_i(t_w^t - t)$:

$$p_i(t_w^t - t) = p_i \left(\underbrace{t_w^i - t}_{\text{recharge time}} + \underbrace{t_w^t - t_w^i}_{\text{translation}} \right). \quad (13)$$

291 This is illustrated on Figure 5 for the three recharge date distributions of Figure 4 translated
 292 to $t_w^t = 2009$. The apparent age determination is modified accordingly:

$$A(t_w^t) = t_w^t - C_{in}^{-1} \left(\int_{-\infty}^{t_w^t} C_{in}(t) p_i(t_w^t - t) dt \right). \quad (14)$$

293 Equation 14 replaces equation 12 and filters out most of the effect of the tracer atmospheric
 294 concentration $C_{in}(t)$ to highlight that of the evolution of the flow pattern. The apparent ages

295 are noted $A(t_w^t)$ recalling that they are obtained after the translation of the recharge date
296 distributions.

297 3.2.2. Results

298 Figure 6 compares the apparent ages obtained with the various recharge date distributions
299 translated to the same sampling date $t_w^t = 2009$ for the model numbered 1. The apparent ages
300 are derived from equation 14 and are noted $A(t_w^t)$. As for the apparent ages from equation 12,
301 the apparent ages $A(t_w^t)$ from equation 14 are first almost identical for the four tracers
302 because of the piston-like shape of the ambient distribution. Because of the broadening of the
303 recharge date distributions after the start of pumping, they diverge from each other to finally
304 reach fixed values spreading over almost 15 years (four last points of Figure 6). The apparent
305 ages $A(t_w^t)$ from the distribution initially sampled at $t_w^i = 1994.1$ (*i.e.* one month after the
306 pumping started) constitute an intermediate case. Indeed, unlike the ages from the ambient
307 distribution, they significantly diverge for the four tracers. However, their spreading is not as
308 broad as for the distributions sampled at later dates ($t_w^i \geq 1995$). We will discuss in section
309 4.1 the interest of these differences for model segregation. We have checked that the
310 conclusions were the same for the other sampling dates of Table 2.

311 3.3. Effect of the temporal evolution of the atmospheric 312 concentration

313 3.3.1. Methodology

314 To assess the influence of the tracer atmospheric concentration $C_{in}(t)$ independently of the
 315 flow pattern modifications, we compute the apparent ages at six translated sampling dates t_w^t
 316 (Table 2) for a fixed recharge date distribution. Figure 7 illustrates this analysis for the pseudo
 317 transient distribution initially sampled at $t_w^3 = 1995$ and translated to 2004 and 2009. This
 318 transformation should not be confounded with the previous one in which we studied the
 319 influence of the recharge date distributions at fixed atmospheric concentration $C_{in}(t)$.

320 3.3.2. Results

321 Figure 8a, b and c display the results for the three distributions of Figure 4a, b and c. For the
 322 ambient distribution (initially arising at $t_w^i = t_w^1 = 1994$), the evolution of $A(t_w^t)$ with t_w^t
 323 remains very small (Figure 8a) because of the restricted dispersion of the recharge date
 324 distribution (blue curve of Figure 4a). It would be strictly equal to zero for a pure piston-flow
 325 model. For broader recharge date distributions corresponding to the pseudo transient case
 326 sampled at $t_w^i = t_w^3 = 1995$ (Figure 8c), the apparent ages strongly evolve with t_w^t . The
 327 weighting of the recharge date distribution progressively evolves with date and yields
 328 different ages consistently with Figure 3. Similar results have been found for the pseudo
 329 transient distributions sampled after t_w^3 (≥ 1995). For the distribution initially sampled one
 330 month after the pumping started (at $t_w^i = 1994.1$), the apparent age variation with t_w^t is still
 331 significant though less important than the age variation from the posterior distributions.

332 In conclusion, the two previous analyses highlight the respective effects of the recharge date
333 distribution (3.2) and of the tracer atmospheric concentration (3.3). They show two well-
334 differentiated regimes of apparent age evolution. The first regime occurs within the first few
335 months after starting the pumping. Note that it is fast in comparison to the mean residence
336 time (50 years). The recharge date distribution shifts from a restricted distribution to an
337 extended one with major consequences on apparent ages. Relatively parallel flow lines under
338 ambient conditions become convergent under pumping inducing the broadening of the
339 recharge date distribution. By comparison, on these short durations (some months), the
340 evolution of the atmospheric concentration has a negligible effect. The second regime occurs
341 after the first year of pumping and lasts for longer period of times. The recharge date
342 distribution marginally changes without any marked effect on the apparent ages. The
343 dominant source of age variation is the non-linear evolution of the tracer atmospheric
344 concentration. This reveals that apparent ages can significantly evolve even if fluid flows and
345 transport are at steady-state. If the second regime is smoother than the first one, it still leads to
346 significant variation of ages (Figure 3).

347 4. Discussion

348 We first discuss the potential interest of the two successive evolutions of apparent ages, *i.e.* a
349 first phase dominated by the transient flow pattern and a second one by the transient
350 atmospheric concentration for flow pattern characterization and models segregation. We
351 secondly compare these modeling results to the available data on the site of Plœmeur.

352 4.1. Information contained in the temporal evolution of apparent 353 ages

354 The temporal evolution of apparent ages contains information on the hydrogeological system,
355 in addition to information contained in the tracer concentrations analyzed at a single time.
356 Yet, information is largely different between the two evolutions identified in sections 3.2 and
357 3.3. The first evolution is the rapid shift when starting pumping from a restricted recharge
358 date distribution to an extended one. The restricted recharge date distribution can be typically
359 fitted by an inverse Gaussian model characterizing mainly the length of the flow paths from
360 the recharge zone divided by the recharge rate (Ginn et al., 2009; Woolfenden and Ginn,
361 2009). The broader recharge date distribution characterizes more globally the aquifer volume
362 and the overall recharge rate (Leray et al., 2012), so does typically the exponential model
363 (Haitjema, 1995). Therefore, almost independent and useful pieces of information, such as a
364 characteristic length *vs.* a volume, can be obtained using the same well before and after the
365 start of pumping. Using equation 12 as an illustration, it comes down to use the temporal
366 evolution of apparent ages to estimate the transient controlling parameters of the function
367 $p(t_w - t)$.

368 Figure 9 compares the temporal evolution of the CFC-12 age for the models numbered 1 and
369 numbered 2 (Table 1) at sampling dates ranging from 1994 to 2009 (Table 2). It shows that
370 the two models give distinct apparent ages before 1995 *i.e.* when the recharge date
371 distribution is transient. Later, once the recharge date distribution is broad and reaches a
372 steady-state, and because the two models have been calibrated on CFC-12 age in 2009, the
373 apparent ages are identical for both models. Differences only occur at short term after the
374 pumping started and result from different transient evolutions of the residence time
375 distribution. This underlines the interest of a continuous sampling of environmental tracer
376 concentrations, particularly at the early times of pumping, to characterize the transient
377 behavior of the system. In that case, apparent age time series can be used as an additional tool

378 to segregate hydrogeological models. Using equation 12 as an illustration, it comes down to
379 use the temporal signal in apparent ages to segregate two functions $p(t_w - t)$ that exhibit
380 distinct transient behaviors.

381 4.2. Comparison to field observations on the site of Plœmeur

382 Apparent ages obtained from CFC-11, CFC-12, CFC-113 and SF₆ data have been determined
383 on the site of Plœmeur since 2006 and recorded in the Plœmeur site database (Ayraud et al.,
384 2008; de Dreuzy et al., 2006). In the pumping well, data are available in 2006 and 2009. CFC-
385 12 age increases from 27.5 in 2006 to 30 years in 2009 and CFC-113 age decreases from 28.5
386 to 26.5 years. CFC-11 ages are close to 45 years and remain constant with time. Still, they
387 should be very close to CFC-12 apparent ages because of the similar normalized atmospheric
388 concentrations of the two tracers. As already reported in Leray et al. (2012), degradation of
389 CFC-11 under anaerobic conditions may explain these differences (Cook and Solomon,
390 1995). SF₆ apparent ages are less than 10 years. Such discrepancies cannot be explained by
391 hydrodynamic mixing alone even at the pumping well (Leray et al., 2012) but are rather
392 coming some geogenic production from the neighboring granites (Busenberg and Plummer,
393 2000; Koh et al., 2007).

394 The results of the models in section 3 suggest that with negligible temporal change of the
395 recharge date distribution, the apparent age should continuously increase whatever the tracer
396 and within the date interval 2000-2010. The CFC-12 age increase at the Plœmeur site is
397 similar in terms of magnitude to that of the models. CFC-12 data thus suggest that the tracer
398 age evolution in that discharge area mainly comes from the temporal evolution of the
399 atmospheric concentration weighting and that the flow pattern and the resulting recharge date
400 distribution in the pumping zone are in turn not expected to vary significantly after 2006.

401 Still, CFC-113 exhibits an opposite age variation in comparison with CFC-12. Considering
402 the age uncertainty due to analytical and sampling errors (Leray et al., 2012), the acquisition
403 of additional concentration data over the next few years would help to confirm the age trends
404 and eventually conclude about the flow pattern stabilization.

405 Earlier flow conditions, and particularly initial ones *i.e.* just before the pumping started, are
406 more difficult to constrain on the site of Plœmeur because of the lack of environmental tracers
407 monitoring before 2006. Contrary to CFCs and SF₆ data, chloride and nitrate concentrations
408 have been monitored on a longer date range starting at 1991. Because of reactivity processes
409 and their evolution with time, the nitrate concentration chronicle can only give partial
410 information on the flow pattern and on mixing processes. However, its non-negligible initial
411 concentration (roughly 15 mg/l) before the start of pumping indicates short residence times
412 consistent with the local recharge area and the short flow paths obtained in the models.
413 Chloride has the advantage of being conservative and being characteristic of deeper waters
414 and thus a good indicator of the flow pattern and its evolution. Figure 10 represents the
415 temporal evolution of chloride concentration at the pumping well. It displays a sharp increase
416 during the first two years of pumping (1st phase of Figure 10), a very slight increase for the
417 next ten years (2nd phase of Figure 10) and finally stabilizes after 2005 (3rd phase of Figure
418 10). The first phase is consistent with the previous modeling result of a quick transition from
419 the piston-like recharge date distribution to the more extended one. The short duration of the
420 first phase is consistent with the fast temporal evolution of the recharge area (Figure 11).
421 Before pumping, the recharge area is a small zone upstream of the well (blue line). It quickly
422 expands to a much larger area around the well only after one year of pumping (green line).
423 Actually, the pumping well collects water that naturally discharged in wetlands next to it and
424 transforms a wide discharge zone to a point-like one.

425 The 2nd phase corresponds to a slight increase of the chloride concentration (Figure 10). This
426 increase does not come from the changes of the recharge area induced by the evolution of the
427 flow pattern, in this case marginal (from orange to purple curves in Figure 11). It more likely
428 comes from the modification of the deep water fraction coming from the main aquifer - *i.e.*
429 the contact zone - that dips quasi-vertically at about 1,500m from the pumping well (Figure
430 11, (Ruelleu et al., 2010)). Its evolution only affects recharge dates earlier than 1940 and
431 cannot consequently be detected by atmospheric gases. Finally, the stabilization of the
432 chloride concentration (3rd phase of Figure 10) agrees with the apparition of a new steady-
433 state regime.

434 5. Conclusion

435 We have analyzed the temporal evolution of apparent ages in a complex aquifer under
436 pumping based on CFCs and SF₆ concentrations measured at the pumping well. The evolution
437 of apparent ages at the pumping well with time can come from (1) the transient nature of flow
438 conditions and (2) the transient evolution of the tracer atmospheric concentrations. To identify
439 the respective role of these two sources, we proposed two successive analyses of the residence
440 time distributions: (1) convolution at the same sampling date (*i.e.* with the same atmospheric
441 concentration chronicle) of residence time distributions initially arising at different dates to
442 assess the effect of the distributions, (2) convolution of one residence time distribution at
443 various sampling dates (*i.e.* with various atmospheric concentration chronicles) to assess the
444 effect of the atmospheric concentration.

445 We identify two well-differentiated phases in the evolution of apparent ages. Apparent ages
446 first evolve because of the pumping-induced modifications of flows. At this stage, the
447 temporal evolution of apparent ages is distinct between two hydrogeological models and may

448 be advantageously used to segregate them using for instance a classical least square
449 comparison procedure of data with modeling results. The transient measure of the tracer
450 concentrations contain some additional information and slightly compensate for the small
451 number of available tracers. After one year of pumping, residence time distributions hardly
452 evolve and apparent ages become solely modified by the transient evolution of the
453 atmospheric concentrations. Apparent ages still significantly evolve but do not contain any
454 additional information on the flow patterns beyond those contained in the steady-state data.

455 Acknowledgments

456 Funding was provided by the French National Research Agency ANR through the H2MNO4
457 project for the development of parallel simulation methods (ANR-11-MN). Research and
458 monitoring on the site of Plœmeur is funded by the Environmental research Observatory H+
459 (Network of hydrogeological sites) and by the European Interreg IV project Climawat. J.-R.
460 de Dreuzy acknowledges the European Union for its additional funding through the IEF
461 Marie-Curie fellowship (PIEF-GA-2009-251710). The authors acknowledge Arash
462 Massoudieh and an anonymous reviewer for their fruitful reviews.

463

464

465 References

- 466 Ayraud, V., 2005. Détermination du temps de résidence des eaux souterraines: application au
467 transfert d'azote dans les aquifères fracturés hétérogènes. Ph.D Thesis, Université de
468 Rennes 1, Rennes, 312 pp.
- 469 Ayraud, V., Aquilina, L., Labasque, T., Pauwels, H., Molenat, J., Pierson-Wickmann, A.-C.,
470 Durand, V., Bour, O., Tarits, C., Le Corre, P., Fourre, E., Merot, P., Davy, P., 2008.
471 Compartmentalization of physical and chemical properties in hard-rock aquifers
472 deduced from chemical and groundwater age analyses. *Applied geochemistry*, 23(9):
473 2686-2707. doi:10.1016/j.apgeochem.2008.06.001.
- 474 Bear, J., 1991. Modelling and applications of transport phenomena in porous media. Theory
475 and applications of transport in porous media. Kluwer Academic Publishers,
476 Dordrecht.
- 477 Bredehoeft, J.D., 2002. The Water Budget Myth Revisited: Why Hydrologists Model.
478 *Groundwater*, 40(4): 340-345.
- 479 Bresciani, E., Davy, P., de Dreuzy, J.-R., 2011. A finite volume approach with local
480 adaptation scheme for the simulation of free surface flow in porous media.
481 *International Journal For Numerical and Analytical Methods in Geomechanics*,
482 36(13): 1574-1591. doi:10.1002/nag.1065.
- 483 Busenberg, E., Plummer, L.N., 2000. Dating young groundwater with sulfur hexafluoride:
484 Natural and anthropogenic sources of sulfur hexafluoride. *Water Resour. Res.*, 36(10):
485 3011-3030. doi:10.1029/2000WR900151.
- 486 Carn, A., 1990. Mise en valeur des ressources en eau souterraine du socle breton. Département
487 du Morbihan (35) - R31724 BRE 4S/90, BRGM, Rennes.
- 488 Castro, M.C., Goblet, P., Ledoux, E., Violette, S., de Marsily, G., 1998. Noble gases as
489 natural tracers of water circulation in the Paris Basin, 2. Calibration of a groundwater
490 flow model using noble gas isotope data. *Water Resour. Res.*, 34(10): 2467-2483.
- 491 Cook, P.G., Love, A.J., Robinson, N.I., Simmons, C.T., 2005. Groundwater ages in fractured
492 rock aquifers. *Journal of Hydrology*, 308(1-4): 284-301.
493 doi:10.1016/j.jhydrol.2004.11.005.
- 494 Cook, P.G., Solomon, D.K., 1995. Transport of atmospheric trace gases to the water table -
495 Implications for groundwater dating with chlorofluorocarbons and krypton-85. *Water*
496 *Resour. Res.*, 31(2): 263-270. doi:10.1029/94WR02232.
- 497 de Dreuzy, J.-R., Beaudoin, A., Erhel, J., 2007. Asymptotic dispersion in 2D heterogeneous
498 porous media determined by parallel numerical simulations *Water Resour. Res.*,
499 43(10). doi:10.1029/2006WR005394.
- 500 de Dreuzy, J.-R., Bodin, J., Le Grand, H., Davy, P., Boulanger, D., Battais, A., Bour, O.,
501 Gouze, P., Porel, G., 2006. General database for ground water site information.
502 *Groundwater*, 44(5): 743-748. doi:10.1111/j.1745-6584.2006.00220.x.
- 503 de Marsily, G., 1986. Quantitative hydrogeology: Groundwater Hydrology for Engineers.
504 Academic Press, New-York, 440 pp.

- 505 Erhel, J., de Dreuzy, J.-R., Bresciani, E., 2008. Multi-parametric intensive stochastic
506 simulations for hydrogeology on a computational grid. In: Tromeur-Dervout, D.,
507 Brenner, G., Emerson, D., Erhel, J. (Eds.), *Parallel Computational Fluid Dynamics*.
508 Springer, Lecture Notes in Computational Science and Engineering, pp. 389-397.
- 509 Erhel, J., de Dreuzy, J.R., Beaudoin, A., Bresciani, E., Tromeur-Dervout, D., 2009. A parallel
510 scientific software for heterogeneous hydrogeology. In: Tuncer, I.H., Gulcat, U.,
511 Emerson, D.R., Matsuno, K. (Eds.), *Parallel Computational Fluid Dynamics 2007*.
512 Lecture Notes in Computational Science and Engineering. Springer, pp. 39-48.
- 513 Frind, E.O., Muhammad, D.S., Molson, J.W., 2005. Delineation of Three-Dimensional Well
514 Capture Zones for Complex Multi-Aquifer Systems. *Groundwater*, 40(6).
515 doi:10.1111/j.1745-6584.2002.tb02545.x.
- 516 Ginn, T.R., Haeri, H., Massoudieh, A., Foglia, L., 2009. Notes on Groundwater Age in
517 Forward and Inverse Modeling. *Transport in Porous Media*, 79(1): 117-134.
518 doi:10.1007/s11242-009-9406-1.
- 519 Haitjema, H.M., 1995. On the residence time distribution in idealized groundwatersheds. *J.*
520 *Hydrol.*, 172(1-4): 127-146. doi:10.1016/0022-1694(95)02732-5.
- 521 IAEA, 2006. Use of chlorofluorocarbons in hydrology : a guidebook. International Atomic
522 Energy Agency, Vienna, 277 pp.
- 523 Kinzelbach, W., 1988. The random-walk method in pollutant transport simulation. In:
524 Custodio, E., Gurgui, A., Lobo Ferreira, J.P. (Eds.), *Groundwater flow and quality*
525 *modelling*. NATO ASI. Dordrecht, New York, pp. 227-246.
- 526 Koh, D.-C., Plummer, L.N., Busenberg, E., Kim, Y.-J., 2007. Evidence for terrigenous SF₆ in
527 groundwater from basaltic aquifers, Jeju Island, Korea : Implications for groundwater
528 dating. *J. Hydrol.*, 339(1-2): 93-104. doi:10.1016/j.jhydrol.2007.03.011.
- 529 Kreft, A., Zuber, A., 1978. On the physical meaning of the dispersion equation and its
530 solution for different initial and boundary conditions. *Chemical Engineering Science*,
531 33(11): 1471-1480. doi:10.1016/0009-2509(78)85196-3.
- 532 LaBolle, E.M., Fogg, G.E., 2001. Role of molecular diffusion in contaminant migration and
533 recovery in an alluvial aquifer system. *Transp. Porous Media*, 42(1-2): 155-179.
534 doi:10.1023/A:1006772716244.
- 535 Le Borgne, T., Bour, O., de Dreuzy, J.-R., Davy, P., Touchard, F., 2004. Equivalent mean
536 flow models for fractured aquifers: Insights from a pumping tests scaling
537 interpretation. *Water Resour. Res.*, 40(3). doi:10.1029/2003WR002436.
- 538 Le Borgne, T., Bour, O., Paillet, J.-L., Caudal, J.-P., 2006. Assessment of preferential flow
539 path connectivity, and hydraulic properties at single-borehole and cross-borehole
540 scales in a fractured aquifer. *J. Hydrol.*, 328(1-2): 347-359.
- 541 Leray, S., de Dreuzy, J.R., Bour, O., Bresciani, E., 2013. Numerical modeling of the
542 productivity of vertical to shallowly dipping fractured zones in crystalline rocks. *J.*
543 *Hydrol.*, 481: 64-75.
- 544 Leray, S., de Dreuzy, J.R., Bour, O., Labasque, T., Aquilina, L., 2012. Contribution of age
545 data to the characterization of complex aquifers. *J. Hydrol.*, 464-465: 54-68.
546 doi:10.1016/j.jhydrol.2012.06.052.

- 547 Long, A.J., Putnam, L.D., 2009. Age-distribution estimation for karst groundwater : Issues of
548 parameterization and complexity in inverse modeling by convolution. *J. Hydrol.*, 376:
549 579-588.
- 550 Maloszewski, P., Zuber, A., 1982. Determining the turnover time of groundwater systems
551 with the aid of environmental tracers, 1. Models and their applicability. *J. Hydrol.*,
552 57(3-4): 207-231.
- 553 McMahan, P.B., Carney, C.P., Poeter, E.P., Peterson, S.M., 2010. Use of geochemical,
554 isotopic, and age tracer data to develop models of groundwater flow for the purpose of
555 water management, northern High Plains aquifer, USA. *Applied geochemistry*, 25:
556 910-922. doi:10.1016/j.apgeochem.20120.04.001.
- 557 Neupauer, R.M., Wilson, J.L., 1999. Adjoint method for obtaining backward-in-time location
558 and travel time probabilities of a conservative groundwater contaminant. *Water*
559 *Resour. Res.*, 35(11): 3389–3398. doi:10.1029/1999WR900190.
- 560 Neupauer, R.M., Wilson, J.L., 2001. Adjoint-derived location and travel time probabilities for
561 a multidimensional groundwater system. *Water Resour. Res.*, 37(6): 1657-1668.
562 doi:10.1029/2000WR900388.
- 563 Neupauer, R.M., Wilson, J.L., 2002. Backward probabilistic model of groundwater
564 contamination in non-uniform and transient flow. *Advances in Water Resources*,
565 25(7): 733-746.
- 566 Nir, A., 1964. On the interpretation of tritium 'Age' measurements of groundwater. *Journal of*
567 *Geophysical Research*, 69(1): 2589-2595.
- 568 Ruelleu, S., Moreau, F., Bour, O., Gapais, D., Martelet, G., 2010. Impact of gently dipping
569 discontinuities on basement aquifer recharge: An example from Plœmeur (Brittany,
570 France). *Journal of Applied Geophysics*, 70(2): 161-168.
571 doi:10.1016/j.jappgeo.2009.12.007.
- 572 Sanford, W.E., Plummer, L.N., McAda, D.P., Bexfield, L.M., Anderholm, S.K., 2004.
573 Hydrochemical tracers in the middle Rio Grande Basin, USA: 2. Calibration of a
574 groundwater-flow model. *Hydrogeol. J.*, 12(4): 389-407. doi:10.1007/s10040-004-
575 0326-4.
- 576 Schwartz, F.W., Sudicky, E.A., McLaren, R.G., Park, Y.-J., Huber, M., Apte, M., 2010.
577 Ambiguous hydraulic heads and ^{14}C activities in transient regional flow. *Groundwater*,
578 48(3): 366-379.
- 579 Sophocleous, M., 2005. Groundwater recharge and sustainability in the high Plains aquifer in
580 Kansas, USA. *Hydrogeol. J.*, 13: 351-365. doi:10.1007/s10040-004-0385-6.
- 581 Stichler, W., Maloszewski, P., Bertleff, B., Watzel, R., 2008. Use of environmental isotopes
582 to define the capture zone of a drinking water supply situated near a dredge lake. *J.*
583 *Hydrol.*, 362: 220-233. doi:10.1016/j.jhydrol.2008.08.024.
- 584 Touchard, F., 1999. Caractérisation hydrogéologique d'un aquifère en socle fracturé : Site de
585 Plœmeur (Morbihan). PhD Thesis, University of Rennes 1, France, 343 pp.
- 586 Trolborg, L., Jensen, K.H., Engesgaard, P., Refsgaard, J.C., Hinsby, K., 2008. Using
587 environmental tracers in modeling flow in a complex shallow aquifer system. *J.*
588 *Hydrol. Eng.*, 13(11): 1037-1048. doi:10.1061/(asce)1084-0699(2008)13:11(1037).

- 589 Waugh, D.W., Hall, T.M., Haine, T.W.N., 2003. Relationships among tracer ages. *Journal of*
590 *Geophysical Research*, 108(C5): 3138. doi:10.1029/2002JC001325.
- 591 Woolfenden, L.R., Ginn, T.R., 2009. Modeled ground water age distributions. *Groundwater*,
592 47(4): 547-557.
- 593 Zhang, Y., 2004. Numerical simulations of dating young groundwater with multiple
594 atmospheric tracers : CFC-11, CFC-12, SF₆, ³H/³He and ⁸⁵Kr. In: Miller, C.T.,
595 Farthing, M.W., Gray, W.G., Pinder, G.F. (Eds.), 15th International Conference on
596 Computational Methods in Water Resources. *Developments in Water Science*.
597 Elsevier Science BV, Chapel Hill, NC, pp. 1367-1378.
- 598 Zinn, B.A., Konikow, L.F., 2007. Potential effects of regional pumpage on groundwater age
599 distribution. *Water Resour. Res.*, 43(6). doi:10.1029/2006WR004865.
- 600 Zuber, A., Rozanski, K., Kania, J., Purtschert, R., 2011. On some methodological problems in
601 the use of environmental tracers to estimate hydrogeologic parameters and to calibrate
602 flow and transport models. *Hydrogeol. J.*, 19: 53-69.

603

604

605 Tables

606 Table 1: Parameters of the two hydrogeological models of the site of Plœmeur used in this
607 study with their reference work. H_{TOT} represents the mean thickness of the aquifer system
608 composed of the micaschists and of the contact zone (Figure 1). The two models have been
609 calibrated on the piezometric level at the pumping well and on CFC-12 apparent age at the
610 pumping well.

611 Table 2 : Sampling dates t_w^i where the apparent ages are determined.

612

613 Figures

614 Figure 1: 3D diagram of the hydrogeological conceptual model composed of the contact zone,
 615 the North 20° normal fault, the micaschists and the two granites. The North 20° normal fault
 616 is underlined by black stripes. The red triangle locates the sampled pumping well. $H(x)$
 617 represents the thickness of the aquifer system composed of the micaschists and the contact
 618 zone. Its mean, noted H_{TOT} , is taken as a proxy for the characterization of its structure. As a
 619 convention, all positions are given in meters and vertical positions are negative below the sea
 620 level and positive above. Adapted from Leray et al. (2012).

621 Figure 2: Boundary conditions applied to the model *i.e.* no flow on the East and the West
 622 boundaries (black lines) and head imposed on the North and South boundaries (red lines). The
 623 limits with the impervious granites are represented by black dashed lines. Discharge zones in
 624 ambient conditions (green) are partly dried with starting the pumping. Specifically, the
 625 wetland in the pumping zone entirely disappears. Figure 3: Apparent ages derived from CFCs
 626 and SF₆ concentrations as functions of the sampling date t_w for the model numbered 1 (Table
 627 1).

628 Figure 4: Recharge date distributions $p(t_w - t)$ of the model numbered 1 (solid curves, left
 629 axis) superimposed on CFC-12 atmospheric concentration $C_{in}(t)$ (grey dashed line, right axis).

630 Recharge date distributions are sampled at: a) t_w^1 (1994 – ambient flow, blue curve), b) t_w^2
 631 (1994.1, wine curve), and c) t_w^3 (1995, green curve). Superposition of the curves shows the
 632 sampling of the tracer atmospheric concentration performed by the recharge date
 633 distributions.

634 Figure 5: CFC-12 atmospheric concentration $C_{in}(t)$ (grey dashes) superimposed on some
 635 translated distributions $p_i(t_w^t - t)$ to the sampling date $t_w^t = 2009$ for the model numbered 1
 636 (Table 1). The translated distributions are the ambient distribution (initially sampled at
 637 $t_w^1 = 1994$, blue curve) and two pseudo transient distributions initially sampled at
 638 $t_w^2 = 1994.1$ (wine curve) and at $t_w^3 = 1995$ (green curve). Note that the ordinate axis has
 639 been broken between 0.05 and 0.19 to display the peak of the ambient distribution.

640 Figure 6: Apparent ages derived from CFCs and SF_6 concentrations for the translated
 641 recharge date distributions $p_i(t_w^i - t)$ with i from 1 to 6 for the model numbered 1 (Table 2).
 642 p_1 corresponds to the blue curve of the Figure 5 (translated ambient distribution), p_2 to the
 643 wine curve of the Figure 5 and p_3 to the green curve of the Figure 5.

644 Figure 7: Recharge date distribution p_3 at its initial sampling date $t_w^3 = 1995$ (green solid
 645 curve) and translated to $t_w^t = 2004$ (green dash dots) and translated to $t_w^t = 2009$ (green
 646 short dashes) for the model numbered 1 (left axis) superimposed on the CFC-12 atmospheric
 647 concentration $C_{in}(t)$ (grey dashed line, right axis)

648 Figure 8: Apparent ages derived from CFCs and SF_6 concentrations as functions of the
 649 translated sampling date t_w^t for the model numbered 1. Apparent ages are obtained for (a) the
 650 translated ambient distribution $p_1(t_w^t - t)$ (blue curve of Figure 4a), (b) the translated

651 pseudo transient distribution $p_2(t_w^t - t)$ (wine curve of Figure 4b) and (c) the translated
652 pseudo transient distribution $p_3(t_w^t - t)$ (green curve of Figure 4c).

653 Figure 9: CFC-12 ages of the model numbered 2 (blue crosses) as a function of CFC-12 ages
654 of the model numbered 1 (Table 1). CFC-12 ages are computed at the pumping well and at
655 sampling dates between 1994 and 2009 (Table 2). Labels next to the crosses stand for the
656 corresponding sampling dates. We recall that the two models have both been calibrated on the
657 CFC-12 age in 2009. Results for the tracers CFC-11, CFC-113 and SF₆ are similar and thus
658 are not shown.

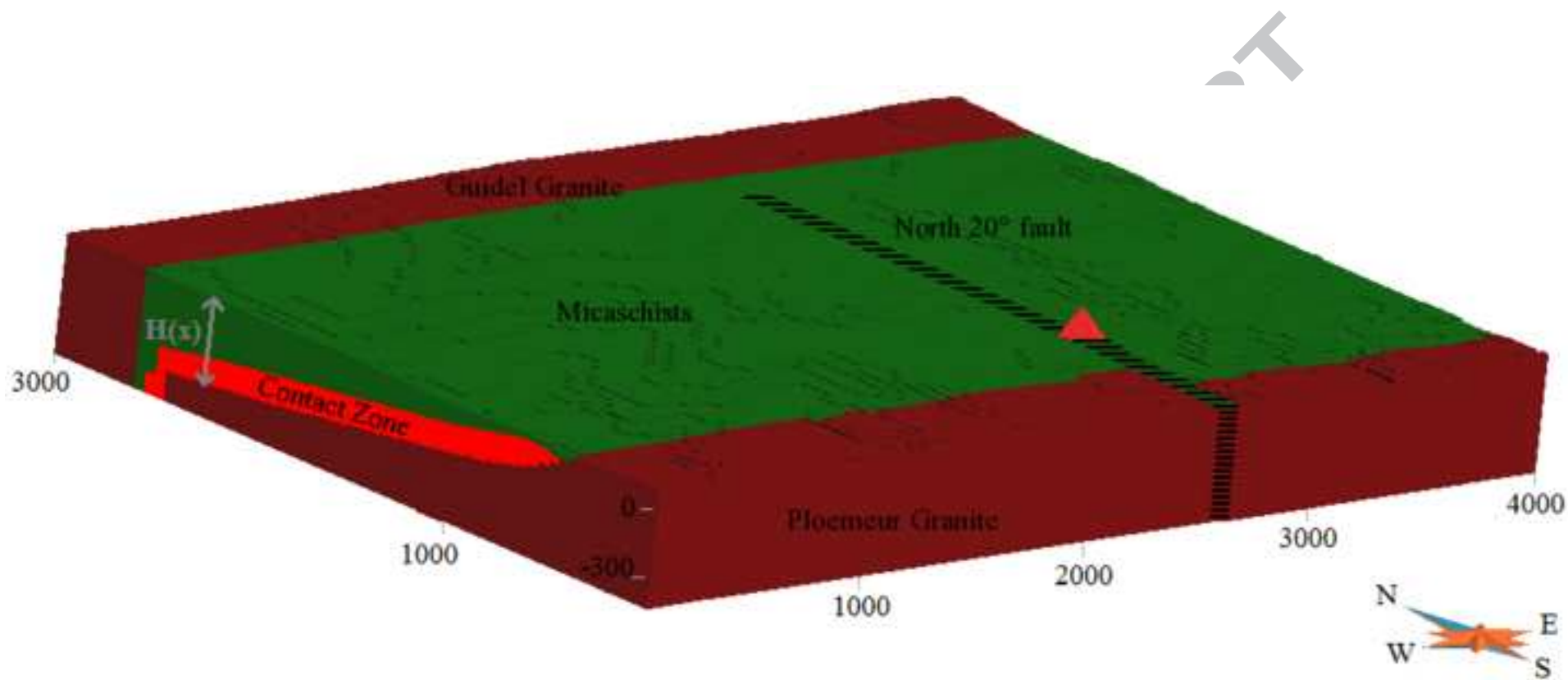
659 Figure 10: Chloride concentration as a function of the sampling date t_w measured at the
660 pumping well of the site of Plœmeur (updated from Ayraud (2005)). The first phase consists
661 in a sharp and fast increase of the chloride concentration, the second phase in a slight increase
662 of the chloride concentration and the third phase in the stabilization of the chloride
663 concentration.

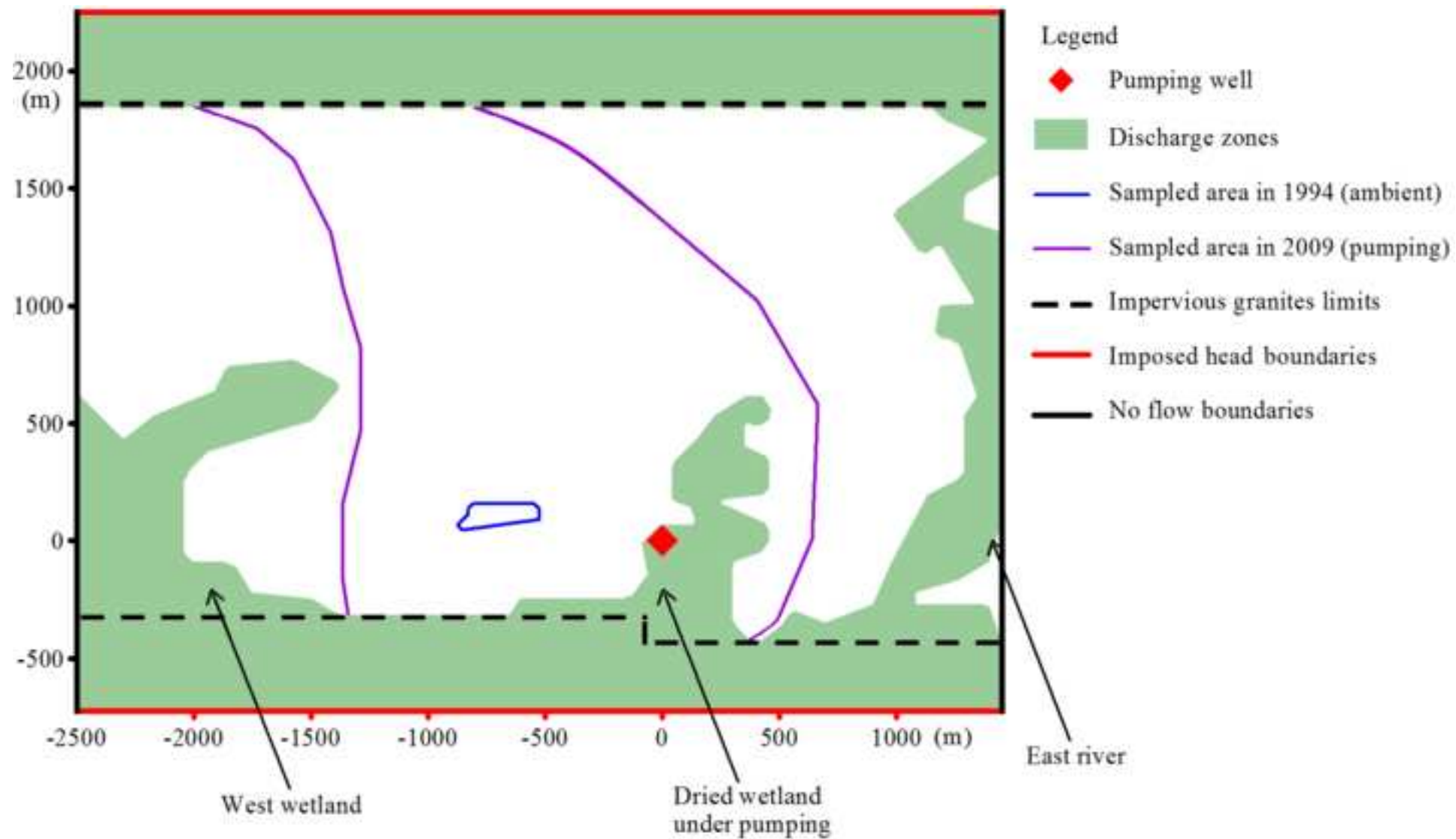
664 Figure 11: Surface origin of the CFCs and SF₆ (corresponding to recharge dates posterior to
665 1940) for the model numbered 1 (Table 1) under pseudo transient conditions sampled at t_w^1
666 (1994 – ambient flow, blue line), at t_w^2 (1994.1, wine line), at t_w^3 (1995, green line), at t_w^4
667 (1999, orange line), at t_w^5 (2004, red line) and at t_w^6 (2009, purple wine).

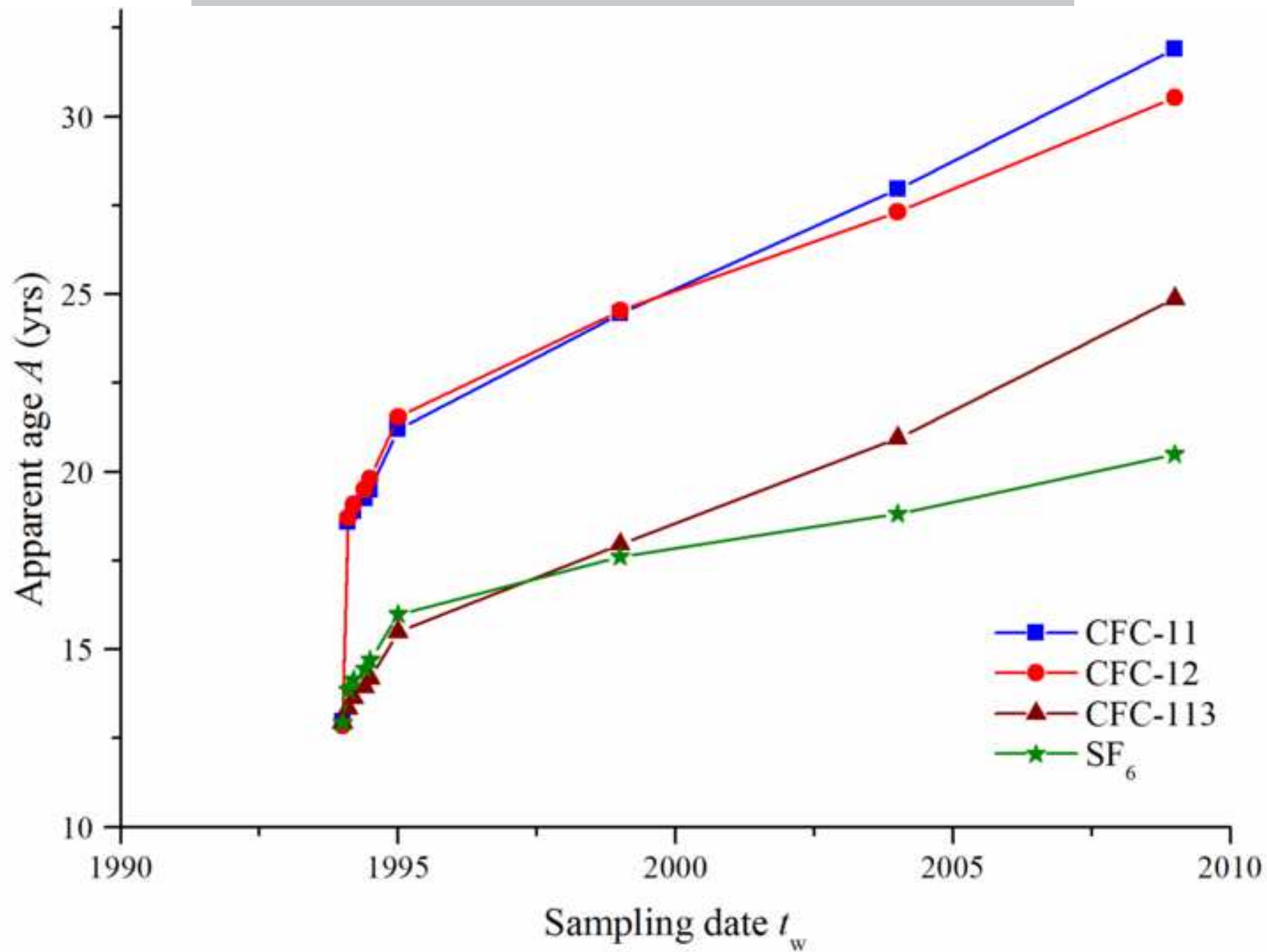
	Values		References
Common parameters			
Potential recharge rate R (mm/year)	200		(Carn, 1990; Touchard, 1999)
Granites conductivity K_G (m/s)	10^{-11}		
Specific parameters for selected models			
	Model n°1	Model n°2	
Mean thickness H_{TOT} (m) – structure name	180 - shallow	280 - deep	(Ruelleu et al., 2010)
Micaschists permeability K_{MS} (m/s)	10^{-6}	5×10^{-6}	(Leray et al., 2012)
Contact zone transmissivity T_{CZ} ($\times 10^{-3}$ m ² /s)	2.27	2.2	(Le Borgne et al., 2004; Le Borgne et al., 2006)
North20° fault transmissivity ($\times 10^{-3}$ m ² /s)	1.14	1.1	(Le Borgne et al., 2004; Le Borgne et al., 2006)
Porosity ϕ (%)	5	2.7	(Leray et al., 2012)

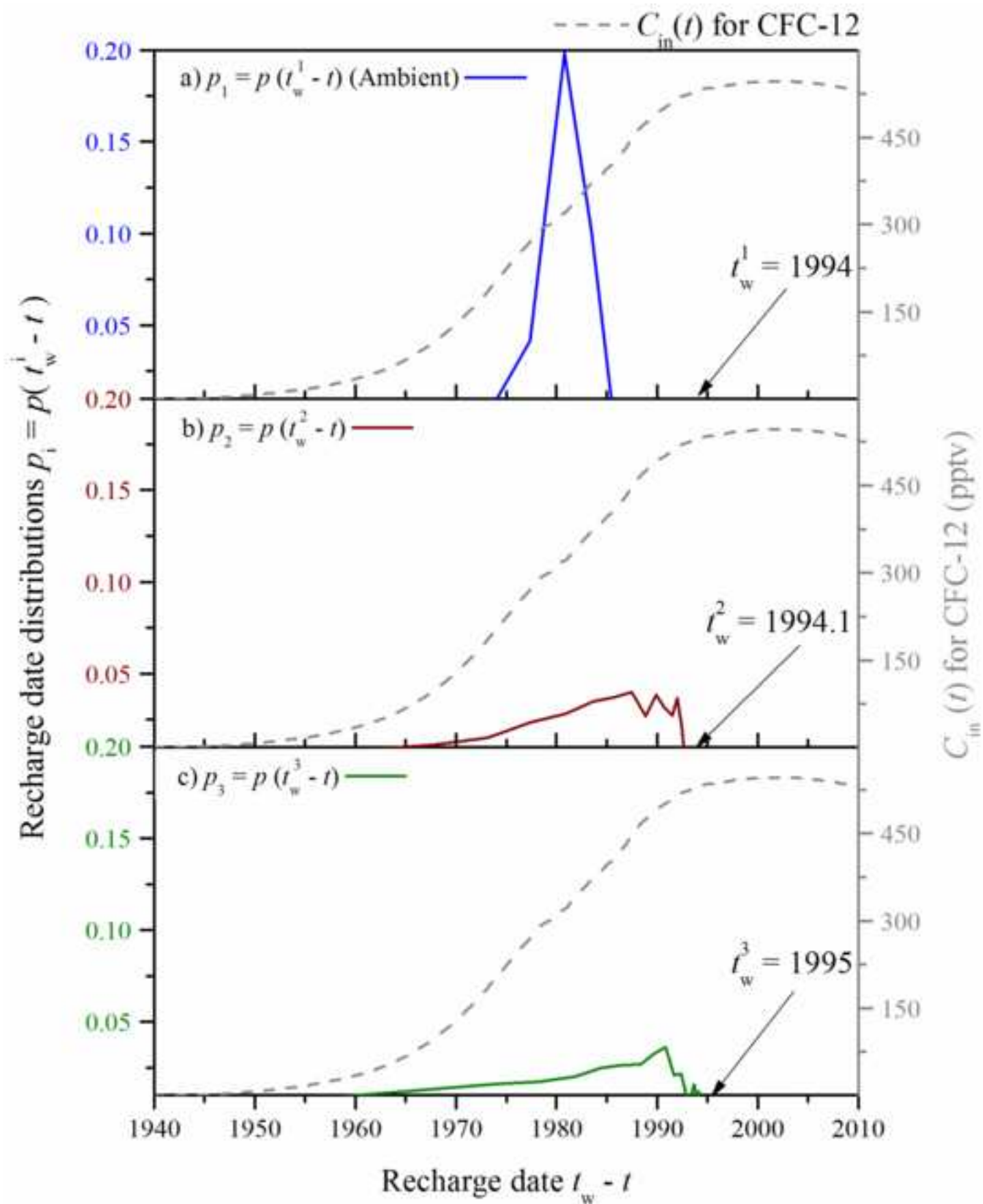
Sampling dates t_w	Acronym	Name and color for corresponding $p(t_w - t)$
1994	t_w^1	$p_1 = p(t_w^1 - t)$, blue
1994.1	t_w^2	$P_2 = p(t_w^2 - t)$, wine
1995	t_w^3	$P_3 = p(t_w^3 - t)$, green
1999	t_w^4	$p_4 = p(t_w^4 - t)$, not displayed
2004	t_w^5	$p_5 = p(t_w^5 - t)$, not displayed
2009	t_w^6	$p_6 = p(t_w^6 - t)$, not displayed

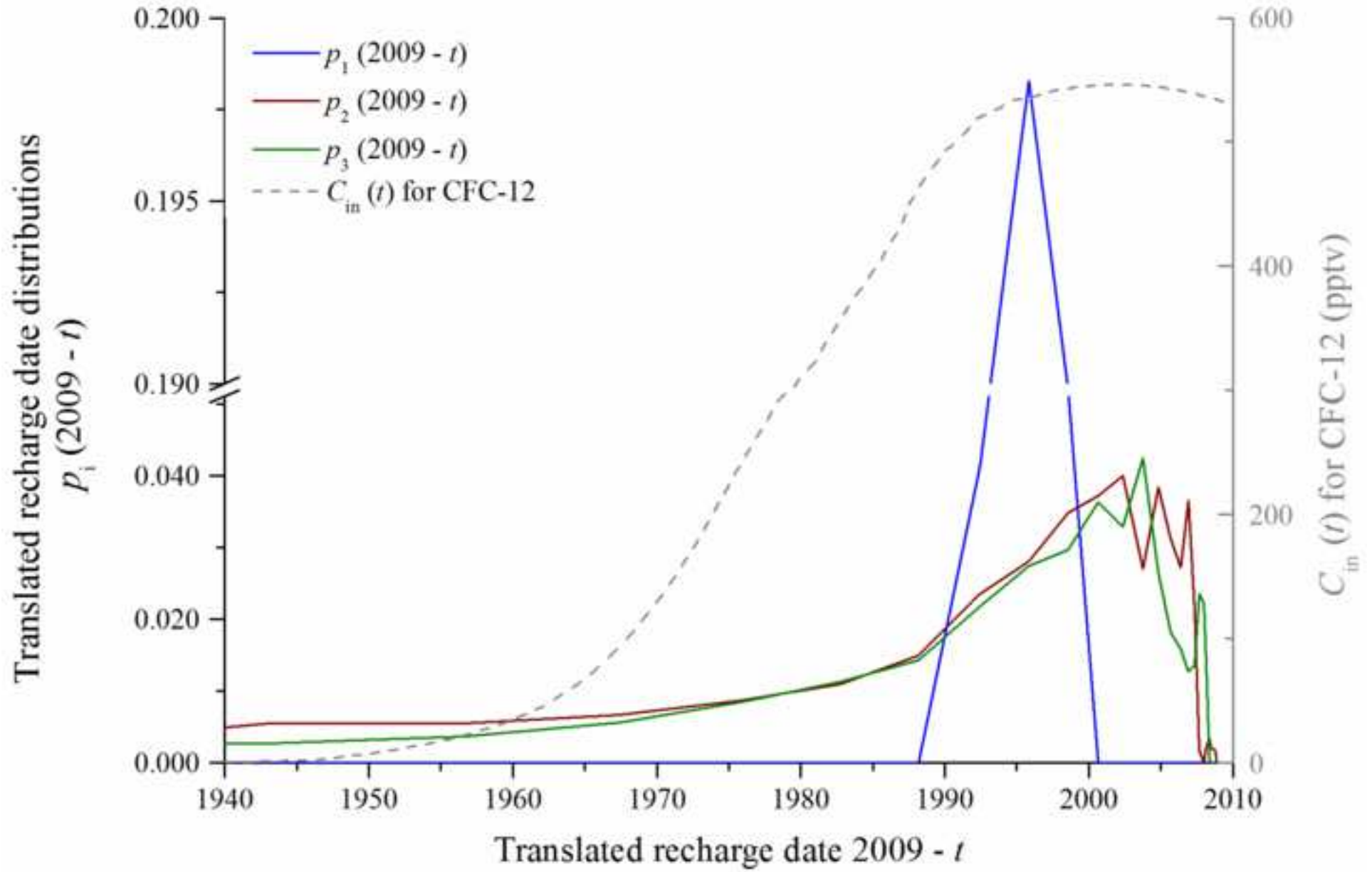
Figure1

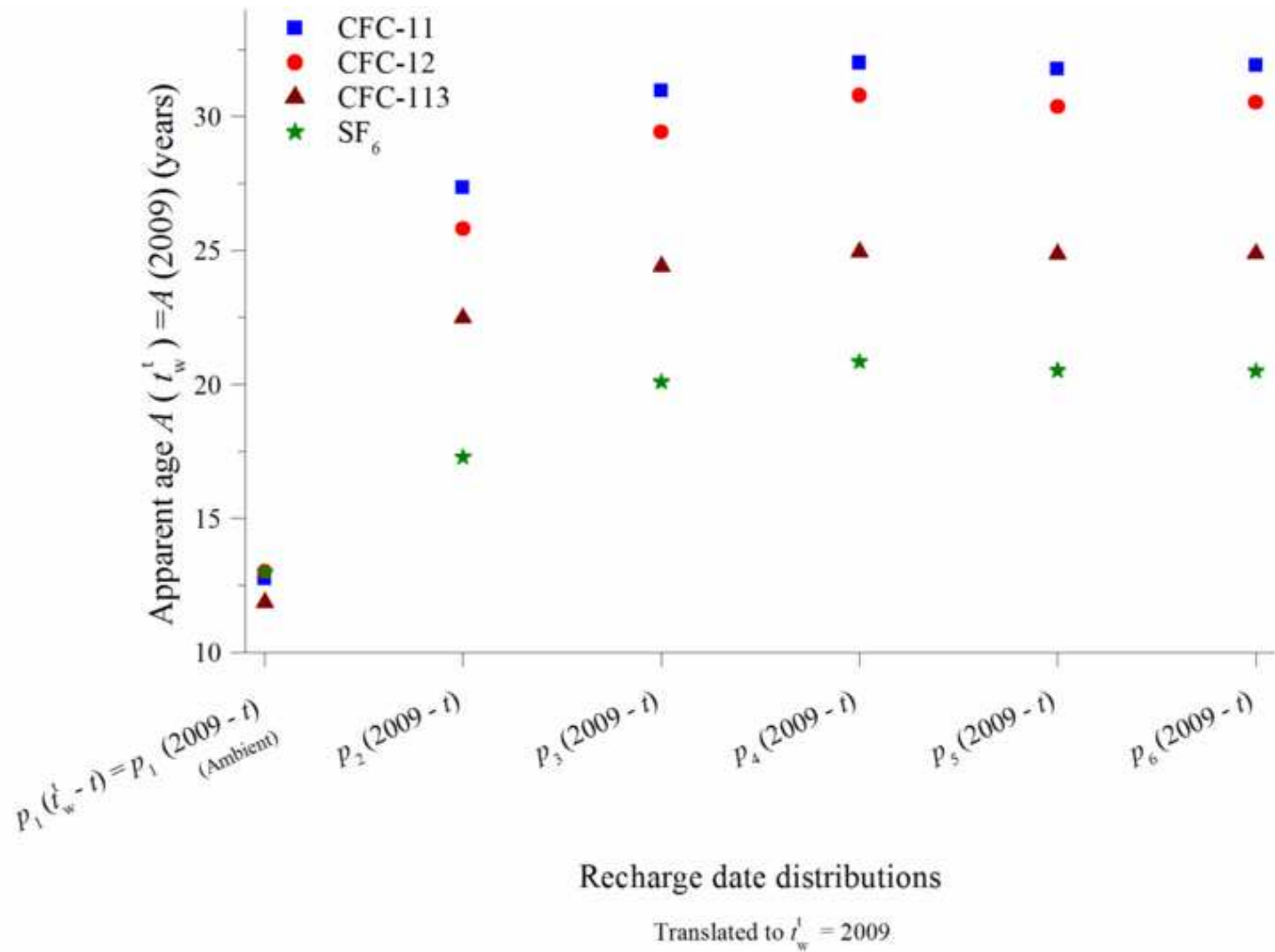


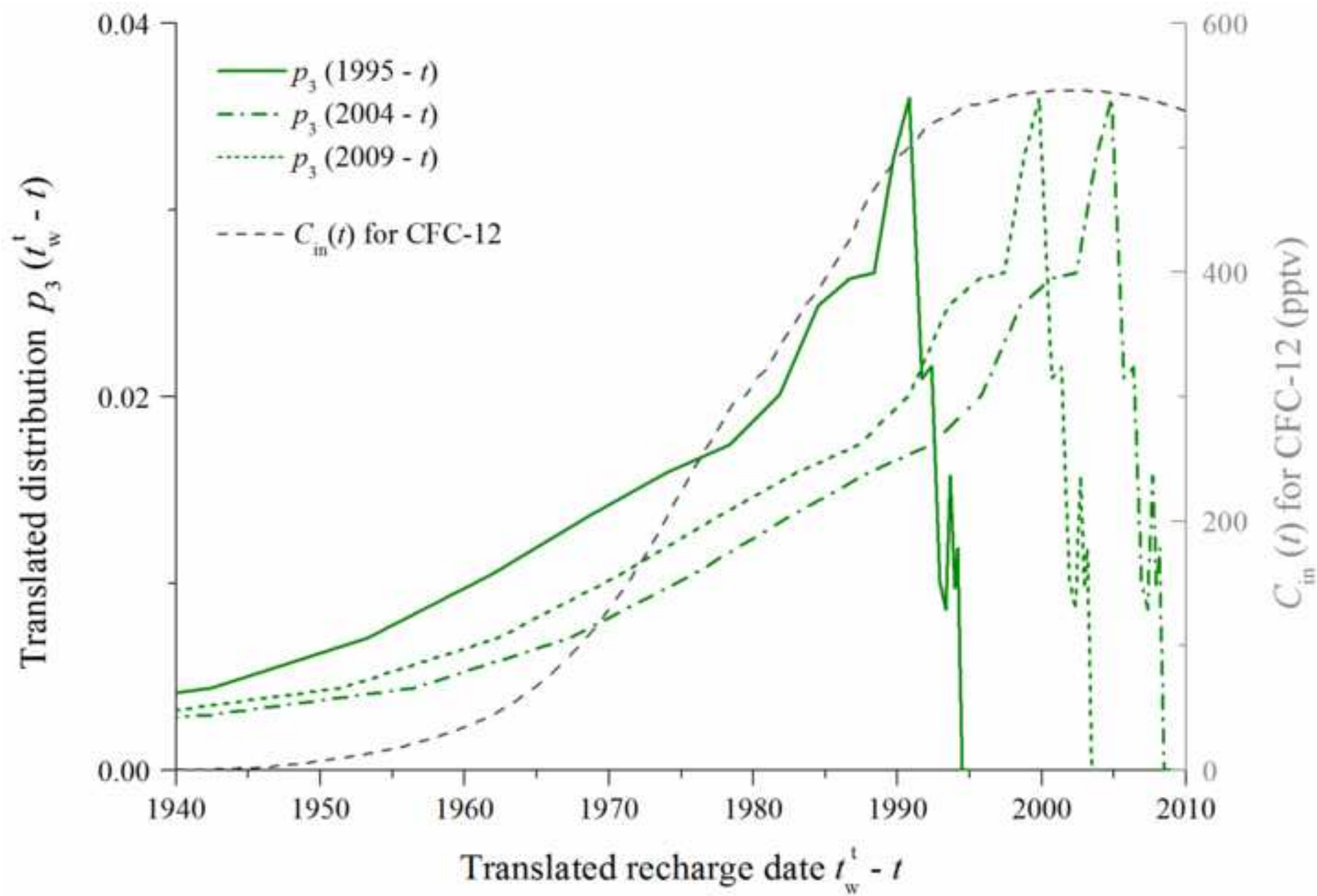


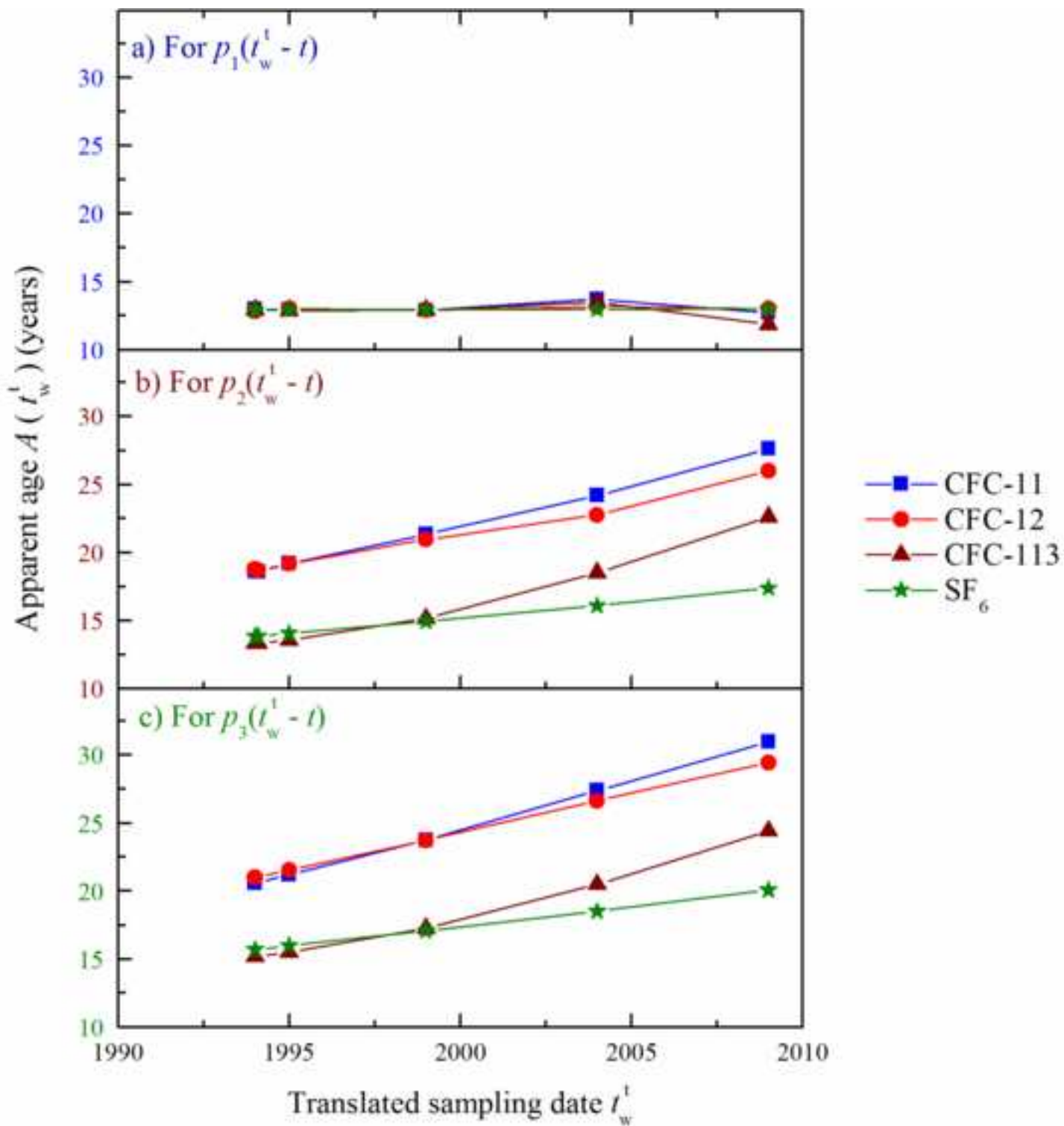












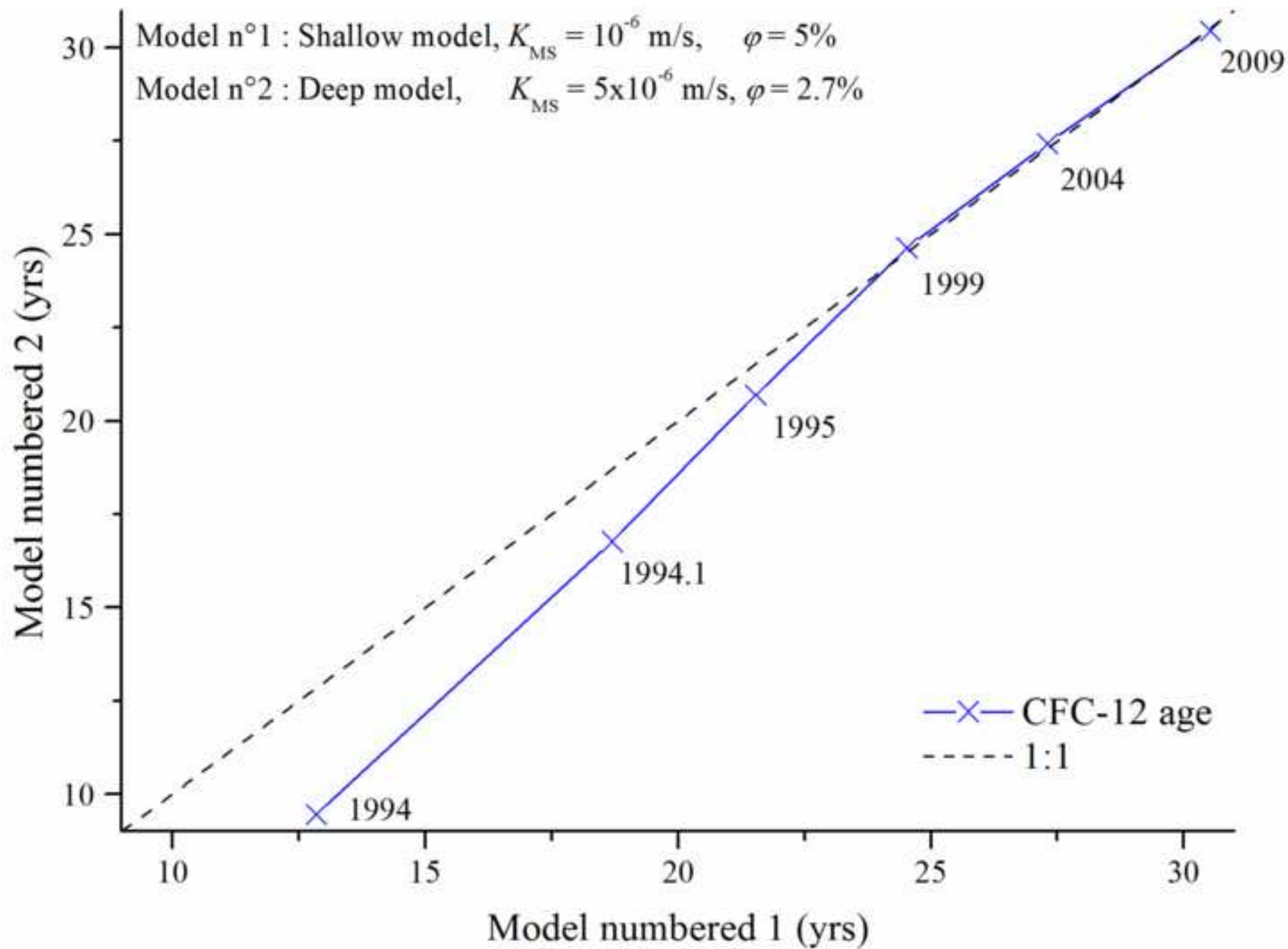
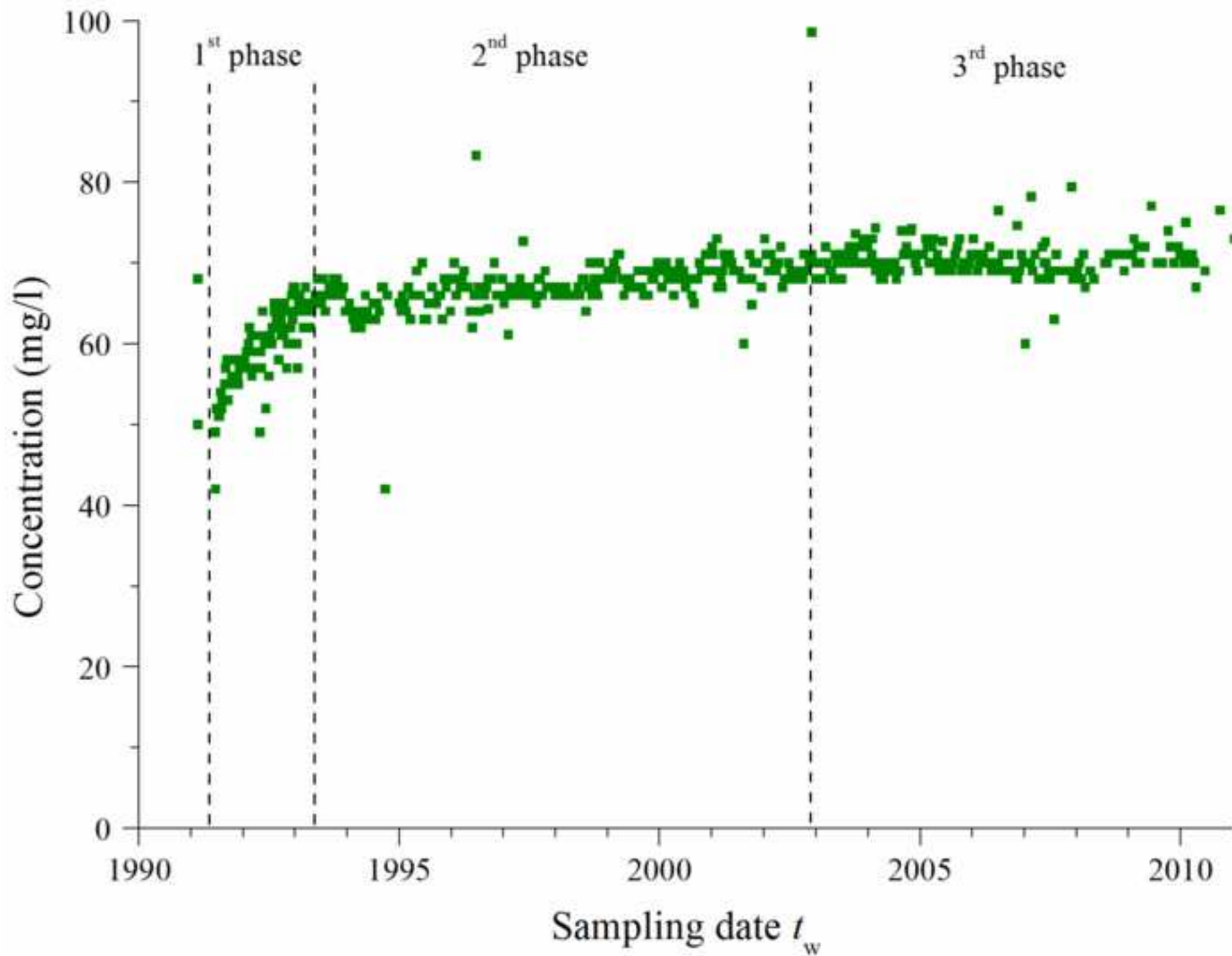
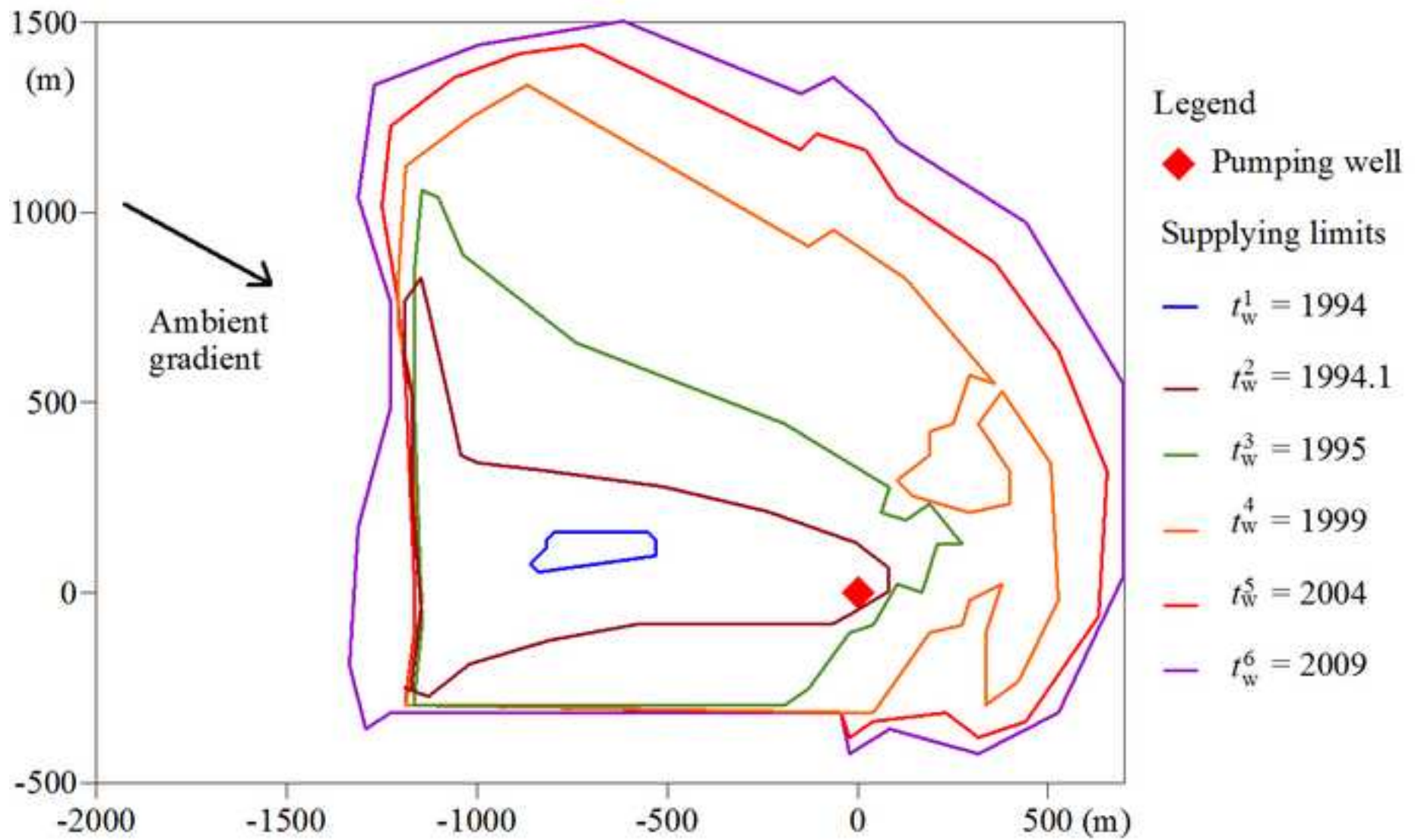


Figure10





Highlights:

- Pumping start is modeled by an immediate shift between two steady-state flow fields
- Ages deduced from CFCs and SF₆ concentrations evolve in two distinct phases
- Transient flow patterns affect ages just after the pumping start but quickly vanish
- Atmospheric concentrations then transiently weight the residence time distribution
- Similar in terms of magnitude, these two regimes are helpful for models segregation